

Solving the nanostructure problem: exemplified on metallic alloy nanoparticles

Valeri Petkov^{a,*}, Binay Prasai^a, Yang Ren^b, Shiyao Shan^c, Jin Luo^c, Pharra Joseph^c and Chuan-Jian Zhong^c

^a *Department of Physics, Central Michigan University, Mt. Pleasant, Michigan 48859, USA FAX: 989 774 2697 Tel: 989 774 3395 E-mail: petko1vg@cmich.edu*

^b *X-ray Science Division, Advanced Photon Source, Argonne National Laboratory, Argonne, Illinois 60439, USA Fax: 630-252-0365 Tel: 630-252-8651 E-mail: yren@anl.gov*

^c *Department of Chemistry, State University of New York at Binghamton, New York 13902, USA Fax: 607-777-4478 Tel: 607-777-4605 E-mail: cjzhong@binghamton.edu*

Supporting Information:

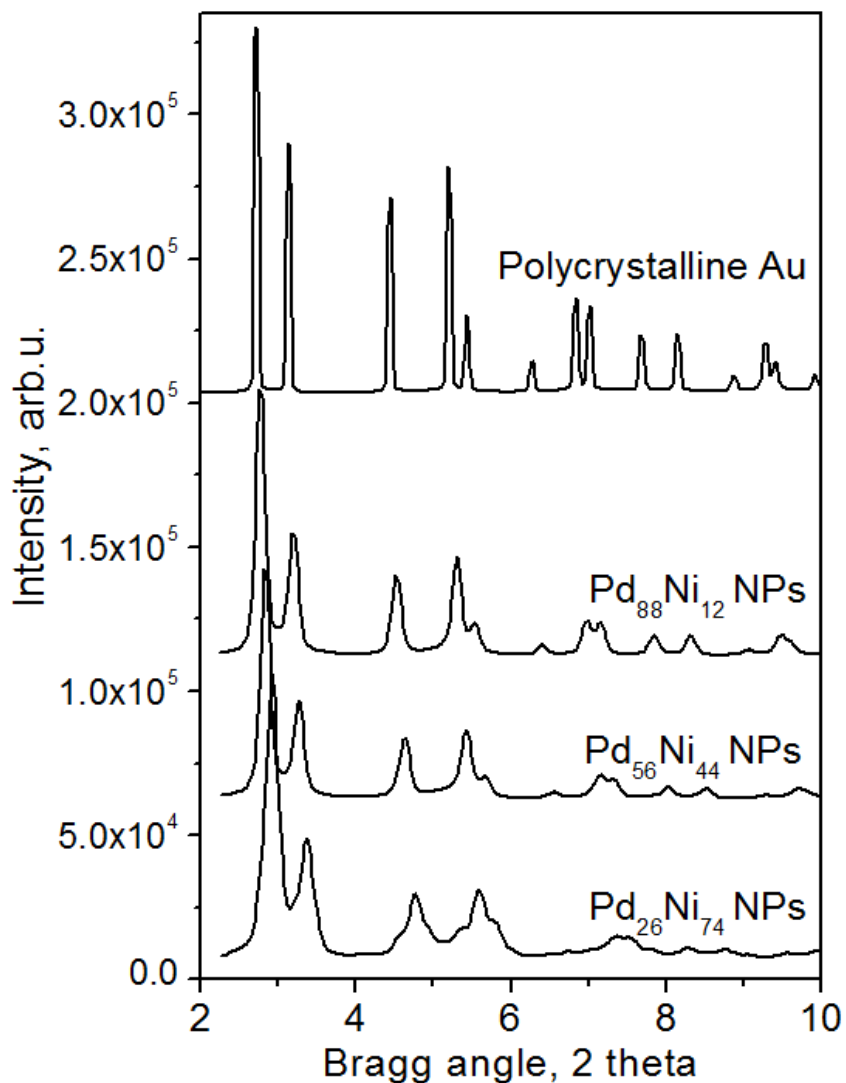


Figure S1: Background & carbon support scattering corrected experimental high-energy synchrotron XRD patterns for Au polycrystalline standard and Pd_xNi_{100-x} NPs. The former shows a series of sharp Bragg peaks while the latter a few broad, Bragg-like features. This renders the well-established, sharp Bragg peaks-based procedures for solving the atomic structure of bulk crystalline materials *technically impossible* to apply to NPs.

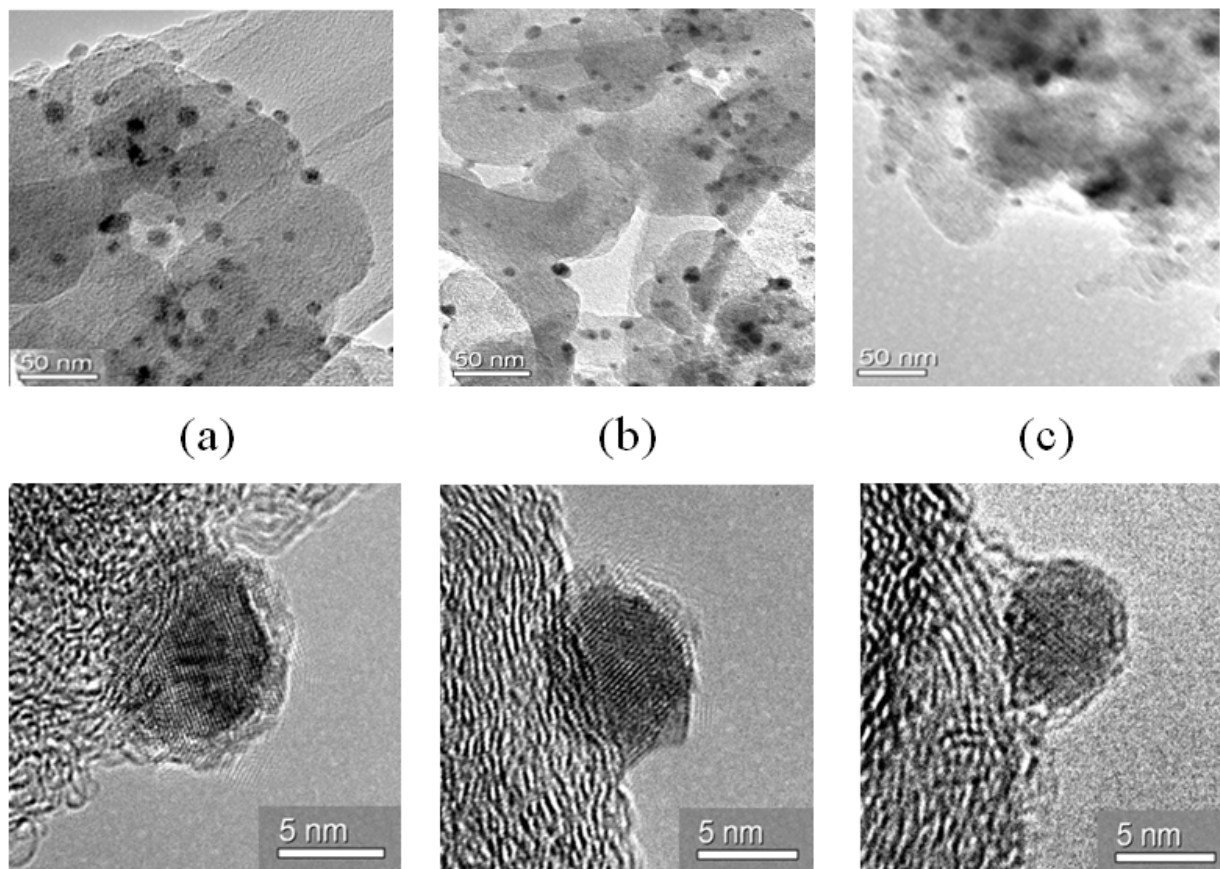


Figure S2. Representative TEM (up) and HR-TEM (down) images of carbon supported $\text{Pd}_x\text{Ni}_{100-x}$ particles (a; $x=26$), (b; $x=56$) and (c; $x=88$) with an average size of 5.0 ± 0.9 nm. Note the “ \pm ” deviations from the average particles size are half widths at full maximum of gaussian-like distribution of sizes extracted from populations of several hundred particles sampled by different TEM images. HR-TEM images show clear lattice fringes inside the NPs. No such are seen close to NP surface indicating the presence of usual NP surface structural disorder.

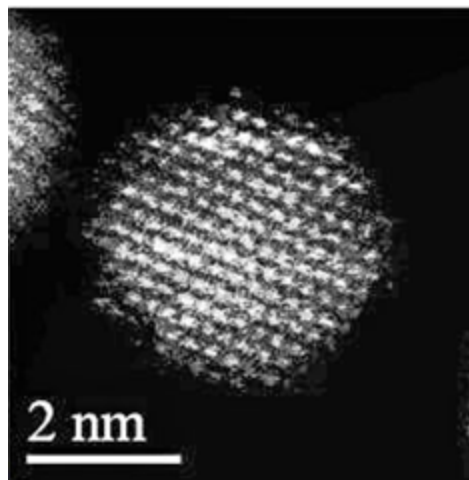
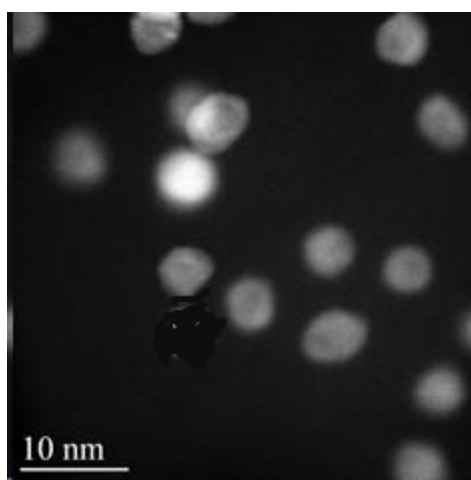


Figure S3. Representative HAADF-STEM image of a collection of Pd₅₆Ni₄₄ NPs. In line with the findings of TEM experiments (see Figure S2 above) HAADF-STEM ones show that Pd₅₆Ni₄₄ NPs are with an average size of 5.0± 0.9 nm (left). Atomic resolution HAADF-STEM image of single Pd₅₆Ni₄₄ NP reveals, in line with HR-TEM images in Figure S2, uneven NP facets indicative of NP surface structural disorder (right).

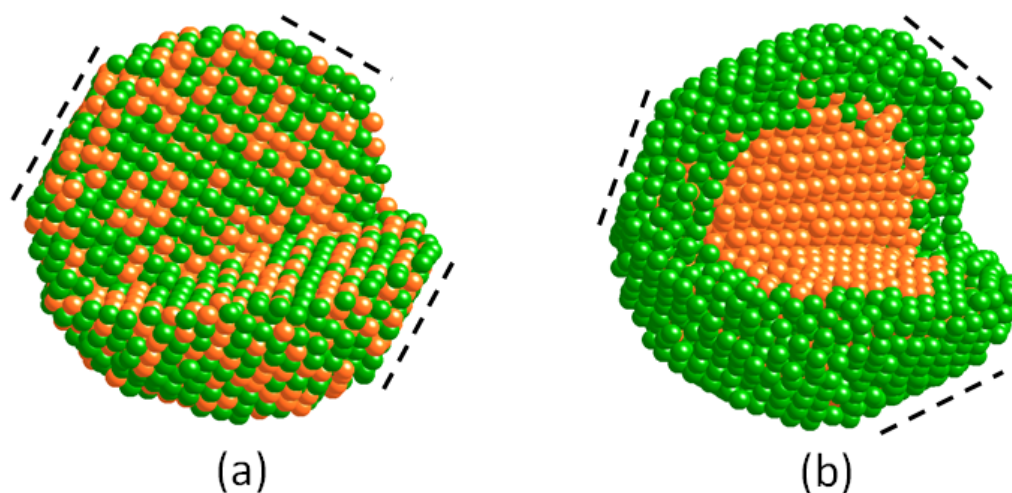


Figure S4. MD optimized structure models for Pd₅₆Ni₄₄ NPs featuring 4100 atom configurations with local fcc-like ordering and distinct random alloy (a) and Ni_{core}-Pd_{shell} (b) patterns. The models are terminated by uniformly flat atomic planes (emphasized by the straight dashed lines). Pd atoms are in green and Ni atoms in orange.

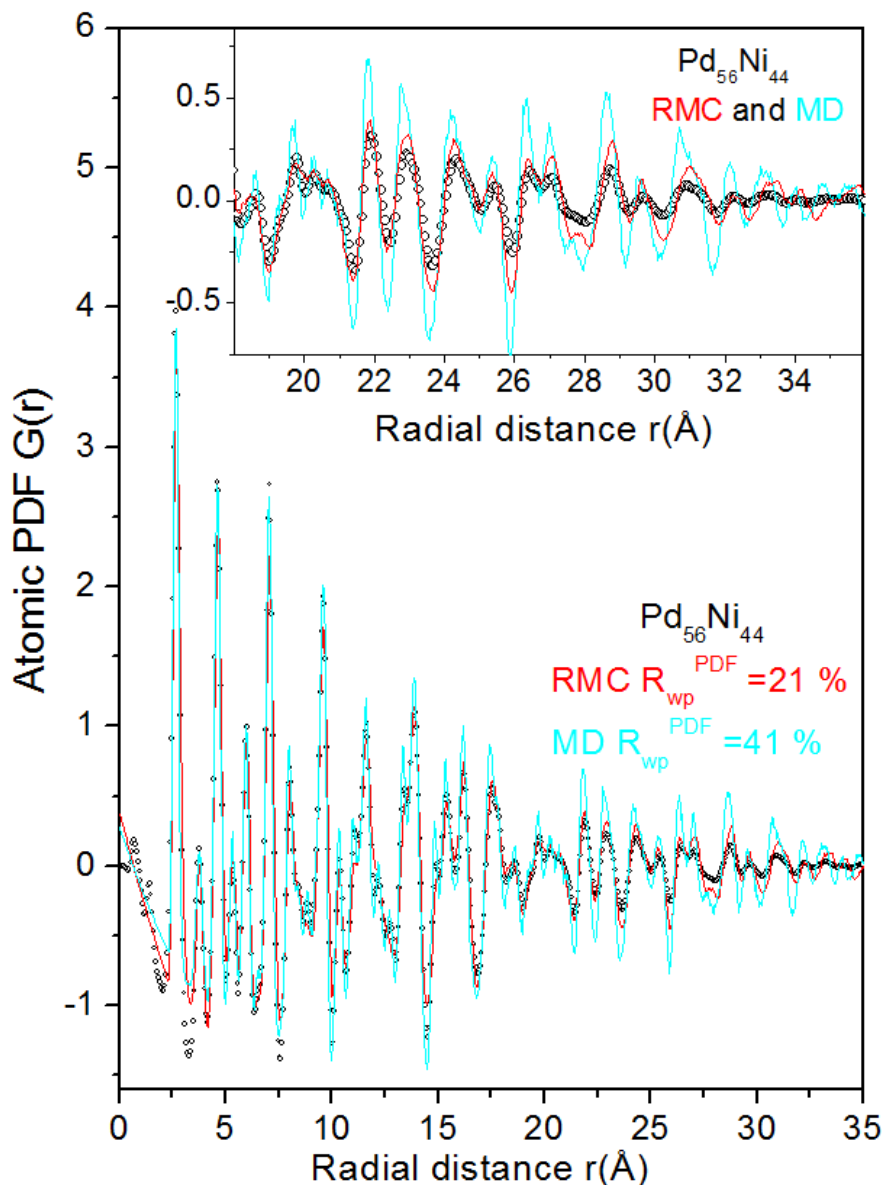


Figure S5. Experimental (symbols) and structure model computed (solid line in cyan) atomic PDFs for Pd₅₆Ni₄₄ NPs. The model (see Fig. S4(a)) has been optimized by MD simulations. Atomic PDF (line in red) computed from the hybrid RMC optimized structure solution for Pd₅₆Ni₄₄ NPs (see Fig. 4(b)) is shown as well. Both the MD optimized structure model and the hybrid RMC optimized structure solution feature 4100 atom configurations with local fcc-like ordering, random alloy chemical pattern and about the same energy. However, as both visual inspection and the respective quality indicators R_{wp}^{PDF} show, the latter reproduces the experimental PDF data in detail while the former does not, especially at longer interatomic distances (see the inset).

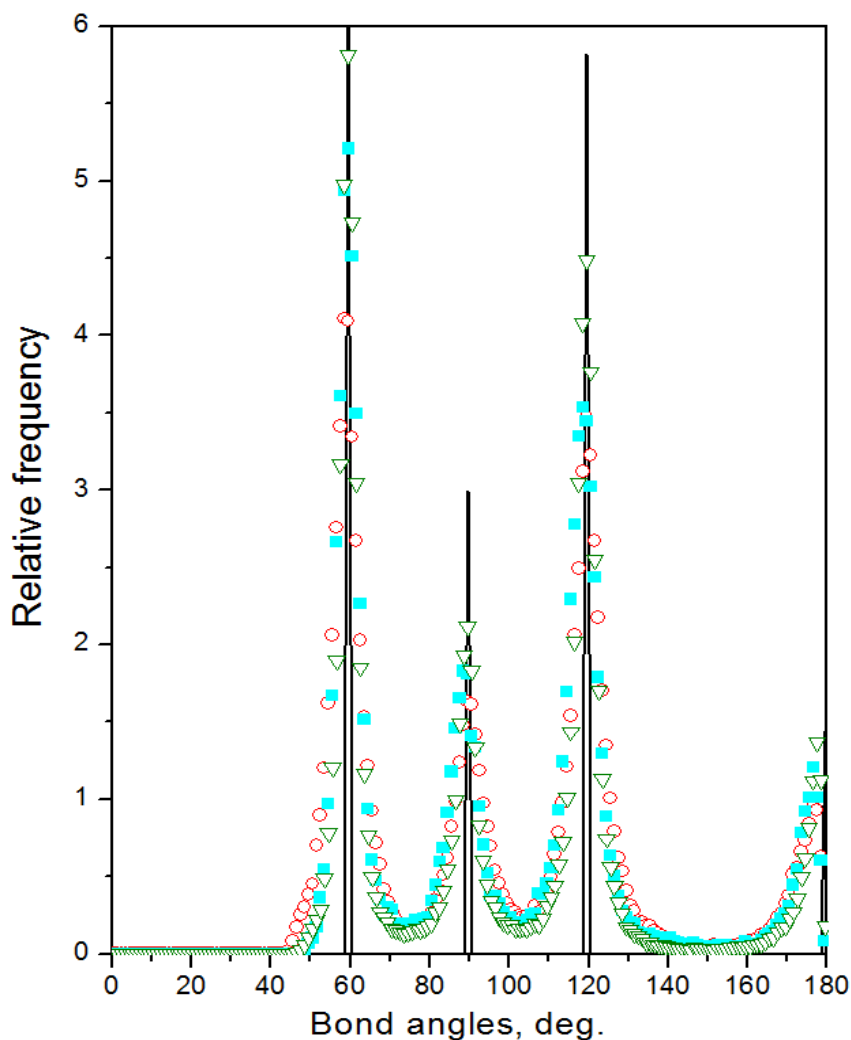


Figure S6. Distribution of bond angles in a 3D periodic fcc-type crystal (lines in black) and in Pd₂₆Ni₇₄ (open circles in red), Pd₅₆Ni₄₄ (full squares in cyan) and Pd₈₈Ni₁₂ (down triangles in green) NPs as derived from the respective NP structure solutions shown in Figure 4. The distribution of bond angles in Pd_xNi_{100-x} NPs is rather broad indicating the presence of significant atomic positional disorder. Yet it appears rather similar to the distribution of bond angles in a 3D periodic fcc-type crystal indicating that, locally, atoms in Pd_xNi_{100-x} NPs are fcc-like arranged.

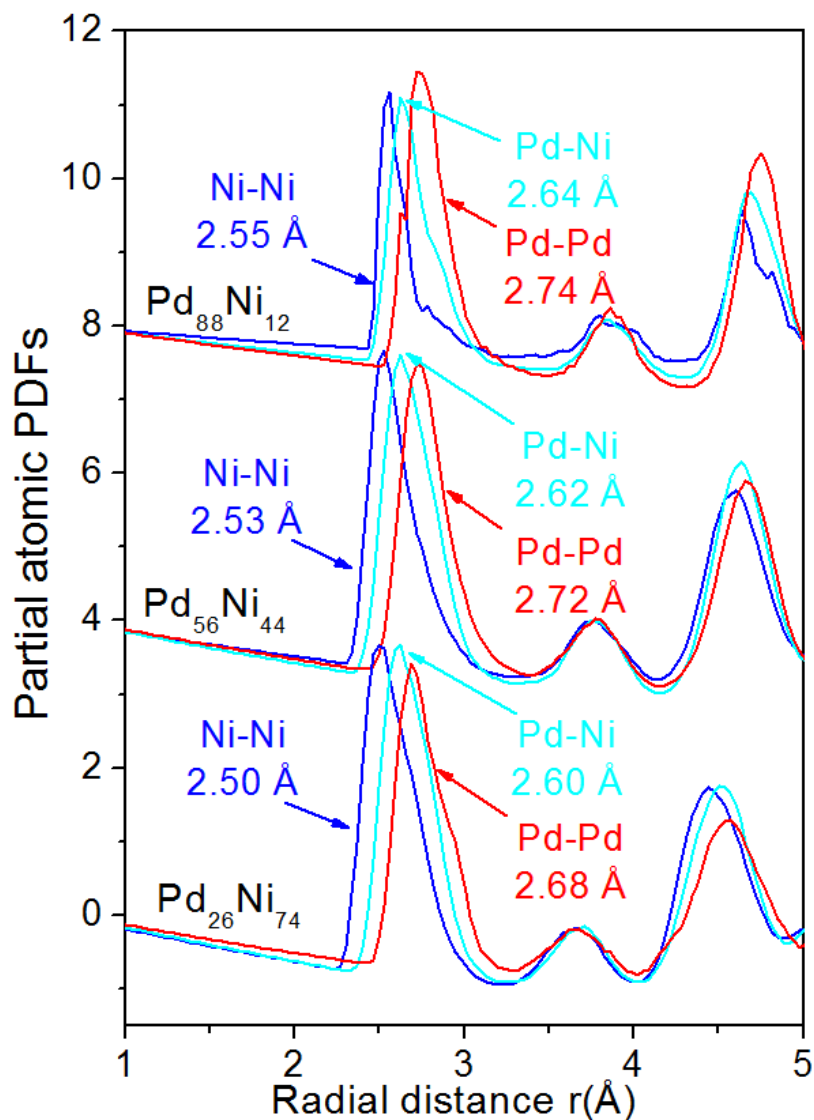


Figure S7. Low-r part of partial atomic PDFs obtained from the structure solutions for Pd_xNi_{100-x} NPs ($x=26, 56$ and 88) shown in Figure 4(a), (b) and (c), respectively. The average first neighbor Ni-Ni, Ni-Pd and Pd-Pd distances, as estimated from the position of the first peak in the respective partial PDFs, are given by each data set (follow the arrows). Partial Ni-Ni, Pd-Ni and Ni-Ni PDFs are in blue, cyan and red, respectively.

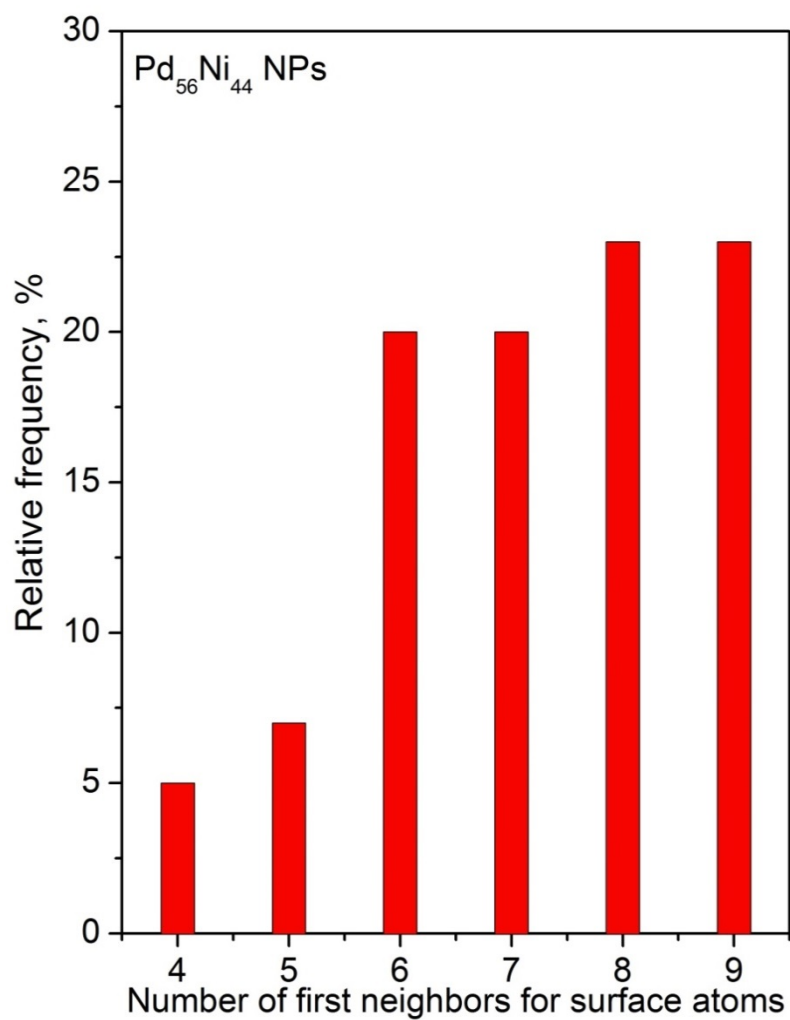


Figure S8. Distribution of total first coordination numbers for atoms sitting at the surface of Pd₅₆Ni₄₄ NPs as derived from the respective structure solution (see Figure 4(b)). The distribution is rather broad indicating the presence of structural disorder at Pd₅₆Ni₄₄ NPs surface.

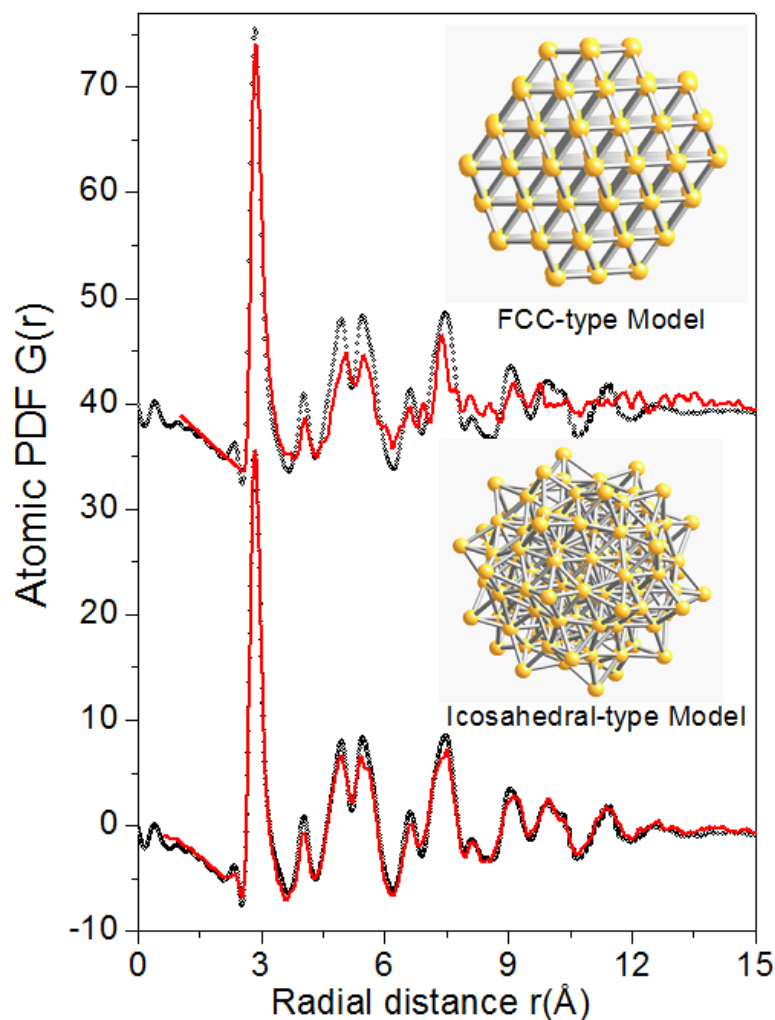


Figure S9. Experimental (symbols) and structure model (line in red) computed PDFs for 144 atom Au NPs. Experimental data are from an assembly of 144 atom particles exhibiting icosahedral-type structure by design. Accordingly, model based on fcc-type structure (up) cannot converge to NP structure solution and so cannot reproduce the experimental PDF data well. On the other hand, model based on icosahedral-type structure (down) converges to NP structure solution easily emphasizing the importance of identifying and using proper NP structure types in solving NP atomic structures. Note bulk Au exhibits fcc and not icosahedral-type structure. Evidently, NP structure type is not necessarily similar to the structure type of the respective bulk counterpart. Ignoring this fact, i.e. assuming that NPs ought to have the structure type of their bulk counterparts and so considering only the latter may turn into a roadblock to solving the “nanostructure problem”. Thanks are due to Dr. Amal Dass from University of Mississippi for providing the experimental PDF data.

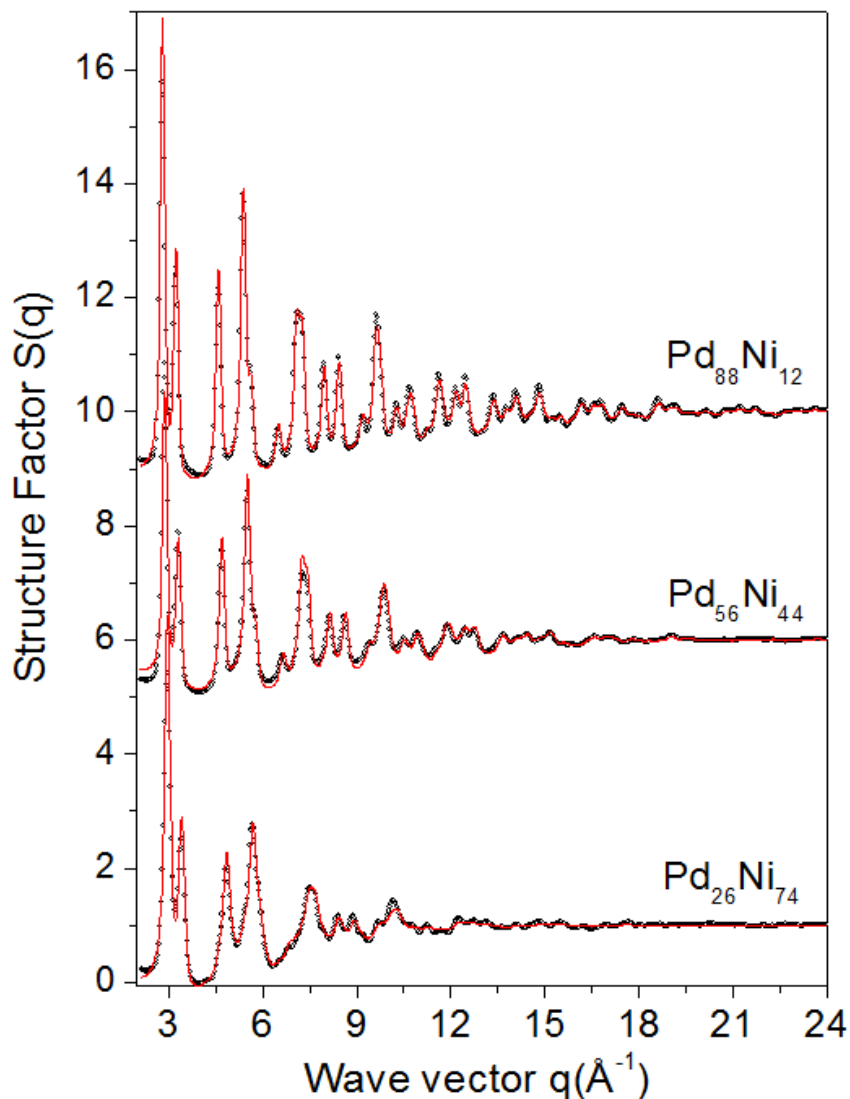


Figure S10. Experimental (symbols) and computed (solid lines in red) structure factors for $\text{Pd}_x\text{Ni}_{100-x}$ NPs ($x=26, 56$ and 88). The computed structure factors are based on the structure solutions shown in Figure 4(a), (b) and (c), respectively. Note, the experimental structure factors $S(q)$ are nothing but the appropriately corrected for experimental artifacts (see the Methods Section) and converted into electron units (see eq. 1) synchrotron high-energy XRD patterns of Figure S1. Good quality NP structure solutions would reproduce not only the experimental atomic PDFs but also the respective $S(q)$ in fine detail, as is the case here. Low quality NP structure solutions may not²⁸. This is to be expected since $S(q)$ s and PDFs are related through Fourier transformation (see eq. 2) which is unitary operation.

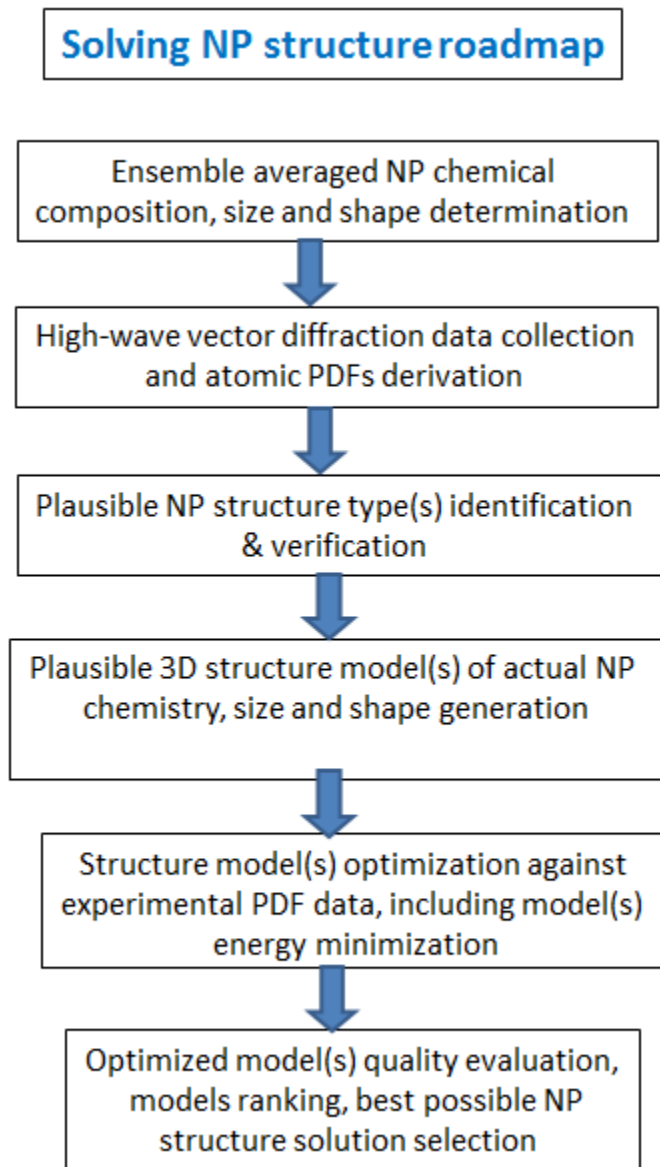


Figure S11. Flowchart of steps to be followed in solving NP atomic-scale structure.